ACS APPLIED MATERIALS & INTERFACES

www.acsami.org

Research Article

Biomimetic Extracellular Matrix Nanofibers Electrospun with Calreticulin Promote Synergistic Activity for Tissue Regeneration

Mary E. Stack, Sarita Mishra, Matangi Parimala Chelvi Ratnamani, Haoyu Wang, Leslie I. Gold,* and Hongjun Wang*

Cite This: https://doi.org/10.1021/acsami.2c13887

Read Online

ACCESS | Metrics & More | Article Recommendations | Supporting Information

ABSTRACT: In recognition of the potential of calreticulin (CRT) protein in enhancing the rate and quality of wound healing in excisional animal wound models, this study was to incorporate CRT via polyblend electrospinning into polycaprolactone (PCL)/type 1 collagen (Col1) nanofibers (NFs; 334 ± 75 nm diameter) as biomimetic extracellular matrices to provide a novel mode of delivery and protection of CRT with enhanced synergistic activities for tissue regeneration. Release kinetic studies using fluoresceinated CRT (CRT-FITC) polyblend NFs showed a burst release within 4 h reaching a plateau at 72 h, with further intervals of release upon incubation with fresh phosphate buffered saline for up to 8 weeks. By measuring fluorescence during the first 4 h of release, CRT-FITC-containing NFs were shown to protect CRT from proteolytic digestion (e.g., by subtilisin) compared to CRT-FITC in solution. CRT incorporated into NFs (CRT-NFs) also showed retention of biological activities and potency for stimulating proliferation and migration of human keratinocytes and fibroblasts. Fibroblasts seeded on CRT-NFs, after 2 days, showed increased amounts of fibronectin, TGF-β1, and integrin β1 in cell lysates by immunoblotting. Compared to NFs without CRT, CRT-NFs supported cell responses consistent with greater cell polarization and increased laminin-5 deposition of keratinocytes and a more motile phenotype of fibroblasts, as suggested by vinculin-capping F-actin fibers nonuniformly located throughout the cell body and the secretion of phosphorylated focal adhesion kinase-enriched migrasomes. Altogether, CRT electrospun into PCL/Col1 NFs retained its structural integrity and biological functions while having additional benefits of customizable loading, protection of CRT from proteolytic degradation, and sustained release of CRT from NFs, coupled with innate physicochemical cues of biomimetic PCL/Col1 NFs. Such synergistic activities have potential for healing recalcitrant wounds such as diabetic foot ulcers.

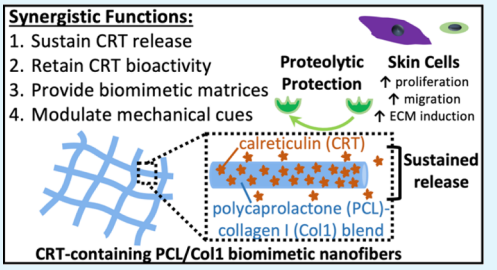

KEYWORDS: *calreticulin, electrospun fibers, proteolytic protection, chronic wounds, fibroblast, keratinocyte, cell migration, cell proliferation*

1. INTRODUCTION

Chronic wounds such as diabetic foot ulcers (DFUs) remain a devastating clinical challenge and cost the U.S. healthcare system over 25 billion dollars annually.[1] It has been estimated that 34% of people diagnosed with diabetes will develop a DFU over their lifetime.[2] DFUs resist most traditional healing treatments, showing a recurrence rate of 65% within 5 years after healing,[2] an amputation rate of 15% within 1 year,[3] and of amputees, a 5 year mortality rate of 40%.[4] Clearly, DFUs present a substantial healthcare burden. Regranex, a gel containing platelet-derived growth factor BB, is the only FDA-approved cytokine treatment for cutaneous wound repair. Although one study showed that 34% of DFUs treated with Regranex healed within 20 weeks,[5] other studies on diabetic mice and treatment of DFUs showed lack of efficacy.[6,7] Conversely, there are many cellular and tissue-based products (CTPs), formerly referred to as skin substitutes, on the U.S. market, but these also display less-than-desirable healing outcomes.[8−10]

Previous work from our group showed that topical application of calreticulin (CRT), an endoplasmic reticulum chaperone protein, markedly enhanced the rate and quality of wound healing in porcine partial-thickness[11] and diabetic mouse full-thickness excisional wounds.[12] In the porcine wounds, CRT-treated wounds were fully reepithelialized with all four layers of epithelium by 10 days post-wounding compared to Regranex-treated wounds, which lacked epithelialization in the center of the wounds. CRT-treated wounds also had greater collagen-rich granulation tissue than the Regranex-treated wounds. Uniquely, CRT healed the diabetic (db/db, lepr null) murine wounds via a tissue regenerative process exemplified by epidermal appendage neogenesis and

Received: August 3, 2022
Accepted: November 1, 2022

lack of scarring. Specifically, thick black pigmented hair and sebaceous glands were regenerated following their complete removal in experimental excisional wounding. In vitro studies using human cells demonstrated that CRT affects key cellular functions essential to the wound healing process including promotion of the migration of keratinocytes, macrophages, and fibroblasts,[11,12] the proliferation of keratinocytes and fibroblasts,[11,12] the synthesis of extracellular matrix (ECM) proteins (e.g., collagen, elastin, and fibronectin) by fibroblasts,[13,14] the upregulation of integrins $\alpha5$ and $\beta1$ by fibroblasts and keratinocytes,[14] and the activation of macrophages to phagocytose debris and release cytokines important to the wound healing process.[13] Clearly, CRT promotes wound healing through diverse and broad-range mediation pathways and can notably correct many of the defects that prevent healing of chronic poor-healing or non-healing and recurrent wounds, such as DFUs.

Electrospun fibers have seen increasing utilities in wound healing, particularly in the repair of animal wound models, as biomimetic ECM substitutes with tailorable physicochemical cues to effectuate cellular responses.[15,16] Polycaprolactone (PCL)- and type I collagen (Col1)-blended or -modified electrospun fibers, in particular, have been studied by our group and others for skin tissue engineering applications.[17−22] The major goal of this study was to combine the beneficial effects of PCL/Col1 nanofibers (NFs) and CRT and thereby create a topical therapeutic with potential to improve poor-healing chronic wounds such as DFUs. CRT was topically applied for 4 consecutive days in the aforementioned porcine and murine wound healing experiments. Notably, repeated topical applications of CRT become essential to maintain the desirable functions, causing unwanted inconvenience in clinical practice and unnecessary consumption of more CRT. Therefore, another objective of electrospinning CRT into PCL/Col1 NFs was to improve delivery of CRT with one application that would have sustained release over time. In addition, for better maintenance of the biological activity of CRT, the structural integrity of the protein needs to be retained despite the challenges of the deteriorated local environment of chronic wounds, which introduce proteolytic[23,24] and pH-unstable[25] conditions. In this regard, it would be highly beneficial to have CRT sustainably released locally while protecting it from these environmental challenges. Other bioactive molecules have demonstrated benefit by being incorporated into drug delivery systems (DDSs).[26−29] In this manner, a final objective of electrospinning CRT into PCL/Col1 NFs was to better protect the structural integrity of CRT against relevant environmental threats.

For these reasons, we sought to determine if PCL/Col1 electrospun fibers could be used as an effective carrier for CRT, particularly with regard to retaining its biological activity, protecting it from proteolytic degradation, and sustaining its release, while at the same time introducing further wound healing capability through the synergy of biological and physicochemical cues. Our results showed that CRT could be uniformly incorporated into PCL/Col1 fibers by direct blending into the electrospinning solution, forming PCL/Col1/CRT (PCC) NFs. Importantly, this blending process neither altered the diameter distribution of obtained NFs nor caused loss of bioactivity of CRT. CRT was able to be sustainably eluted from these NFs under physiological conditions [37 °C in pH 7.4 phosphate buffered saline (PBS)] and was persistently present within NFs as long as last measured at 8 weeks. Upon challenge by enzymatic exposure, CRT in NFs exhibited greater resistance to proteolytic degradation. With a clear trend though not statistically significant, PCC NFs retained the function of inducing fibroblast migration in in vitro wound healing gap closure assays. In comparison, PCC NFs stimulated significantly faster keratinocyte migration and more complete gap closure. Furthermore, PCC NFs elicited a migratory cell phenotype represented by cell polarization and laminin-5 deposition by keratinocytes and cell polarization, vinculin-capped F-actin fibers, and phosphorylated focal adhesion kinase (pFAK) localization in fibroblasts. PCC NFs also promoted proliferation of both fibroblasts and keratinocytes. In addition, PCC NFs upregulated the synthesis of transforming growth factor (TGF)-$\beta1$, a key protein involved in upregulation of ECM proteins and integrin $\beta1$ receptor involved in migration. Taken together, PCC hybrid NFs exhibit potential for healing recalcitrant wounds such as DFUs with a synergistic action that is not observed with PCL/Col1 NFs or with CRT alone.

2. MATERIALS AND METHODS

2.1. Materials. Recombinant human CRT expressed in *Escherichia coli* was obtained from Intas Pharmaceuticals Ltd. (Ahmedabad, India) and used from a 6.4 mg/mL stock solution in Tris-Ca buffer (TC; 10 mM Tris, 3 mM $CaCl_2$, pH 7.0). For selected experiments, CRT was fluorescently tagged with fluorescein isothiocyanate isomer I (FITC, from Sigma-Aldrich) under basic conditions to obtain CRT-FITC.[30] Glass coverslips and calcium chloride solution (1.0 M) were obtained from Carolina Biological Supply Company. Tris buffer solution (2 M) and sodium carbonate were purchased from Acros Organics. Collagen type I (Col1, lyophilized from calf skin) was from Elastin Products Company. 1,1,1,3,3,3-Hexafluoro-2-propanol (HFIP) was obtained from Oakwood Products. Polycaprolactone (PCL, average Mn 80 kDa), branched polyethylenimine (BPEI, average Mw 750 kDa), mitomycin C [10 mg/mL in dimethyl sulfoxide (DMSO)], and sodium bicarbonate were obtained from Sigma-Aldrich. Elastase from human neutrophils, cathepsin G from human neutrophils, proteinase K from *Tritirachium album*, and subtilisin A from *Bacillus licheniformis* were purchased from MilliporeSigma and reconstituted per the manufacturer's protocol. All cell culture media and additives were from Gibco with the exception of keratinocyte basal medium (KBM, Lonza), L-glutamine (Corning), fetal bovine serum (FBS, Atlanta Biologicals), and trypsin−ethylenediamine tetraacetic acid for primary cells and trypsin neutralizing solution from the American Type Culture Collection (ATCC).

2.2. Fabrication and Characterization of CRT-Containing Fibrous Matrices. Glass coverslips were cleaned with isopropanol and then coated with BPEI (0.2 mg/mL, pH 9) for 20 min and blotted dry to improve subsequent adherence of electrospun fibers. NF matrices were prepared using an established electrospinning technique with modification.[31,32] Briefly, PCL and Col1 (3:1 w/w) dissolved in HFIP overnight at 4 °C were mixed with CRT/TC solution at a volume ratio of 7:3 for 1 h at 4 °C under stirring (final polymer concentration of 10% w/v PCL/solvent). The final concentrations of CRT in various polyblend electrospinning solutions are shown in Table 1. For the study of CRT release kinetics and stability in the presence of enzymes, CRT-FITC was similarly electrospun into NFs (PCCf-100n). Upon loading into a 1 mL syringe with a 21G stainless steel blunt-tip needle, the electrospinning solution was dispensed at a flow rate of 0.6 mL/h through an electric field of 1 kV/cm to fabricate NFs, which were collected onto the BPEI-coated glass coverslips on top of ground aluminum foil. A 4 min collection time was chosen to assure sufficient NF coverage of the glass coverslips. Ambient conditions during electrospinning were 10−58% relative humidity and 20.5−27.9 °C temperature. The morphology of various NF matrices was examined by scanning

https://doi.org/10.1021/acsami.2c13887
ACS Appl. Mater. Interfaces XXXX, XXX, XXX−XXX

Table 1. Design of CRT-Containing PCL/Col1 Nanofiber (NF) Matrices[a]

designated abbreviation of NF matrices	CRT concentration in electrospinning solution	anticipated CRT concentration releasable from NFs
PCX	none	none
PCC-1μ	900 μg/mL	1 μg/mL
PCC-100n	90 μg/mL	100 ng/mL
PCC-10n	9 μg/mL	10 ng/mL
PCC-1n	900 ng/mL	1 ng/mL
PCC-100p	90 ng/mL	100 pg/mL
PCC-1p	900 pg/mL	1 pg/mL

[a]CRT, calreticulin; PCL, polycaprolactone; Col1, type I collagen; PCX, PCL/Col1; PCC, PCL/Col1/CRT.

electron microscopy (SEM; Zeiss Auriga Small Dual-Beam Field Emission) with a voltage of 1 kV and a working distance of approximately 5 mm. Fiber diameters were determined by using ImageJ to measure 50 fibers across 5 randomly selected SEM fields. Localization of CRT-FITC within NF matrices was examined with an EVOS M7000 Imaging System (Thermo Fisher Scientific).

2.3. CRT Release from CRT-Containing NFs. Release experiments were performed with 15 mm-diameter PCX and PCCf-100n NF samples inside a 24-well plate with receiver volumes of 700 μL of PBS each. Plates were sealed with a plate sealer and wrapped in parafilm and aluminum foil to prevent evaporation and light exposure followed by incubation at 37 °C. At designated timepoints, a 70 μL sample (i.e., 10%) was removed from each well and replaced with fresh PBS to maintain a constant receiver volume. The fluorescence intensity of these samples was immediately recorded with a BioTek Synergy H1 Microplate Reader through a green filter and used to calculate the cumulative mass of CRT-FITC released from the NFs against a standard curve. For prolonged release studies, the receiver volume was completely replenished (i.e., 100%) with fresh PBS every 2−5 days, and the NF matrices were also imaged immediately after submerging in fresh PBS with an EVOS M7000 Imaging System (Thermo Fisher Scientific).

2.4. Proteolytic Resistance of CRT-Containing NFs. To examine the susceptibility of CRT to proteolytic degradation following electrospinning into NFs, CRT-FITC (free) or PCCf-100n (CRT-FITC incorporated into NFs) was subjected to treatment with elastase, subtilisin, cathepsin G, and proteinase K separately. CRT-FITC/PBS solution (3.1 nM) or 15 mm-diameter PCCf-100n samples submerged in PBS were incubated with elastase or cathepsin G at a molar ratio of 1:10 or with subtilisin or proteinase K at a weight ratio of 1:10 or 1:100 (enzyme/CRT), and the reaction was carried out under static conditions at 37 °C. Starting at 15 min and then every 20 min thereafter, a sample of the supernatant was collected followed by measuring its fluorescence intensity using a BioTek Synergy Neo2 Hybrid Multi-Mode Microplate Reader (excitation wavelength: 485 nm, emission wavelength: 528 nm). After 275 min, the reaction was terminated by addition of 1 mM phenylmethylsulfonyl fluoride. The data were expressed as fold change in fluorescence intensity of the sample (free CRT-FITC or PCCf-100n) with or without enzyme treatment at 275 min to fluorescence intensity of the same sample type without enzyme treatment at 15 min referred as CRT initial (CRTi).

2.5. Cell Culture. Primary human neonatal foreskin fibroblasts (HFF; CRL-2091, CCD-1070Sk, ATCC) were cultured in complete minimum essential medium (MEM) containing 10% FBS, 2 mM L-glutamine, 1 mM sodium pyruvate, 50 IU/mL penicillin, and 50 μg/mL streptomycin with medium refreshed every 3−4 days. Cells were passaged at 60−70% confluency and used for experiments at passages 8−11. Telomerase-immortalized human keratinocytes (HEKs), a past gift from Dr. James Rheinwald (NIH Harvard Skin Disease Research Center), were cultured in complete keratinocyte serum-free medium (KSF) containing 50 μg/mL bovine pituitary extract (BPE), 5 ng/mL epidermal growth factor (EGF), and 0.3 mM additional $CaCl_2$, 100 IU/mL penicillin, and 100 μg/mL streptomycin with medium refreshed every 2−3 days. Cells were passaged at 50−60% confluency. All cellular experiments on NFs were performed using 22 × 22 mm samples with the exception of the wound healing gap closure assay which was performed using 15 mm-diameter samples. All NF samples were sterilized using ultraviolet irradiation (20 min per side) prior to use, and all treatment media contained 1% TC to equalize the effects of the exogenous CRT vehicle.

2.6. Resazurin Assay for Cell Proliferation. To evaluate proliferation, cells were seeded onto NF matrices in a 6-well plate or directly onto tissue culture plastic (TCP) of a 96-well plate. For HFFs, cells were seeded at a density of 5.7×10^3 cells/cm^2 and allowed to adhere for 6−8 h prior to further treatment. Complete MEM medium with reduced FBS (i.e., 0.5%) was used to minimize the contribution of serum, except for the FBS positive control (i.e., PCX-FBS with 5% FBS). Conditioned medium (CM) refers to medium containing released CRT that was obtained by soaking PCC-100n NFs in FBS-reduced complete medium for 1 day and, respectively, diluted 10-fold and 100-fold with fresh FBS-reduced complete medium to obtain the estimated CRT concentrations of 10 and 1 ng/mL. For HEKs, cells were seeded at a density of 1.0×10^4 cells/cm^2 and allowed to adhere overnight prior to further treatment. Complete KSF medium was used throughout the experiment. For groups with exogenous CRT treatment, cells were seeded on PCX NFs, and then, CRT was supplemented into the medium to reach the designated concentration (e.g., 10 ng/mL for the PCX-10n group). At predetermined timepoints, resazurin (Biotium) was mixed with either 0.5% FBS-complete MEM (for HFFs) or KBM (for HEKs) at a 1:9 volume ratio and then incubated with cells (1 mL/well). After an appropriate incubation period, 100 μL of the supernatant from each well was transferred to a 96-well plate, and the absorbance at 570 and 600 nm was recorded using the BioTek Synergy H1 Microplate Reader. The net absorbance of each sample at each timepoint was normalized to the average value of the negative control at the initial timepoint in order to determine proliferation.

2.7. Cell Motility Assay. To evaluate motogenic capacity, samples of NF matrices on glass coverslips were secured inside wells of a six-well plate.[30] HFFs were seeded at a density of 5.7×10^3 cells/cm^2 and allowed to adhere for 6 h prior to various treatments using 0.5% FBS-complete MEM. Immediately following treatment, samples were automatically imaged every 20 min for the next 12 h using a BioTek Cytation C10 Confocal Imaging Reader. Acquired images were analyzed in ImageJ. Boolean OR and subtraction operators were first used to attenuate the NF background and identify individual cells, and the Manual Tracking plugin in ImageJ[33] was used to track 10 cells per condition.

2.8. Wound-Gap Closure Assay. To further evaluate motogenic capacity, a wound-gap closure analysis was performed with both HFFs and HEKs on NF matrices. Briefly, samples of NF matrices on glass coverslips were secured inside wells of a 24-well plate.[30] To better monitor the gap closure, cells were labeled with Vybrant DiD (Invitrogen) according to the manufacturer's instructions (15 min for HFFs, 10 min for HEKs). CytoSelect Wound Healing Assay inserts (Cell Biolabs, Inc.) were used to create a wound gap of 0.9 mm on the surface of each NF sample; cells were seeded onto each side of the insert (4.5×10^4 per side for HFFs, 1.0×10^5 per side for HEKs) and allowed to adhere overnight. Immediately upon removal of the inserts, the cells were treated with mitomycin C (5 μg/mL, 1 h) to block proliferation (n.b. so that migration of cells observed would not be due to proliferation into the wound gap). Then, the cells were incubated in respective treatment medium (0.5% FBS-complete MEM for HFFs, complete KSF without BPE and EGF for HEKs), and gap closure was monitored periodically by imaging with the EVOS M7000 Imaging System (Thermo Fisher Scientific). Gap closure with DiD labeling was analyzed in ImageJ. First, red channel images of the full surface (stitched using EVOS M7000 software) at different timepoints were aligned using the StackReg plugin available in ImageJ[34] and cropped to the area of interest. Then, gap area was quantified using a macro based on a previous report,[35] and the gap closure was quantified as a percent relative to the initial timepoint. In some

https://doi.org/10.1021/acsami.2c13887
ACS Appl. Mater. Interfaces XXXX, XXX, XXX−XXX

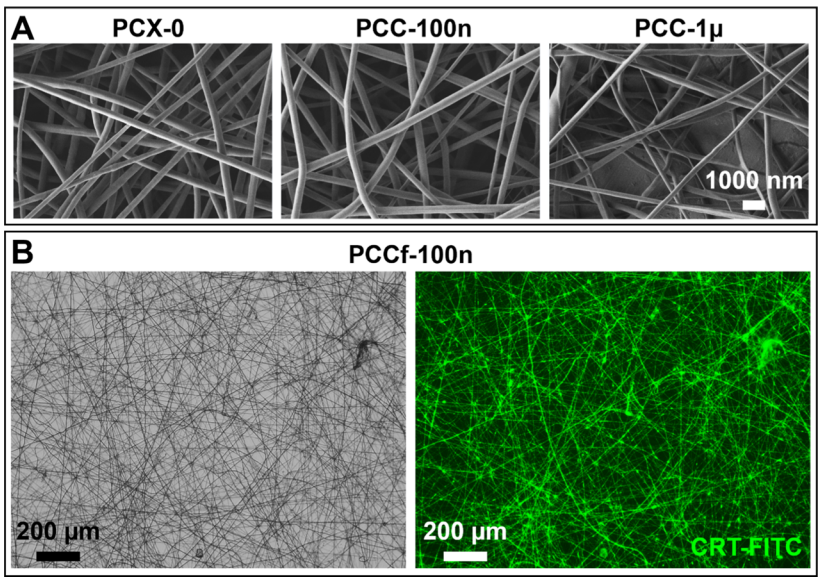

Figure 1. Incorporation of CRT into PCL/Col1 NFs. (A) SEM images of PCX-0, PCC-100n, and PCC-1μ NFs. (B) Matching brightfield and fluorescence images of PCCf-100 NFs taken in the same field of view and magnification. Green fluorescence is CRT-FITC.

experiments where DiD-labeling and mitomycin C pretreatment was not used per our previously published method,[32] the culture was fixed at the designated time, and then, the cells were stained with methylene blue (0.25 mg/mL, 15 min) and imaged using the EVOS M7000 Imaging System.

2.9. Immunofluorescent Staining. Cultures were fixed with 4% paraformaldehyde for 10 min at room temperature and stored in PBS at 4 °C until use. Cells were then permeabilized with 0.1% Triton X-100 for 5 min and blocked for nonspecific binding with 3% w/v bovine serum albumin (BSA)/PBS for 5 min. All antibodies were diluted in 3% w/v BSA, and the primary or secondary antibody incubation was performed at room temperature for 1 h with gentle shaking. Primary antibodies used were as follows: rabbit anti-phosphorylated FAK (anti-pFAK; Abcam, 1:400), mouse anti-keratin-1/10 (K1/10; Santa Cruz Biotechnology, 1:50), mouse anti-laminin-5 (EMD Millipore, 1:200), FITC-conjugated mouse anti-vinculin (Sigma-Aldrich, 1:100), FITC-conjugated mouse anti-Ki67 (Santa Cruz Biotechnology, 1:50), Texas Red-conjugated phalloidin (Biotium, 1:100), and Alexa Fluor 488-conjugated phalloidin (Invitrogen, 1:200). All conjugated secondary antibodies were from Jackson ImmunoResearch (1:50−1:100). Immediately following staining, samples were washed with PBS, mounted with 4,6-diamidino-2-phenylindole (DAPI), and sealed with clear nail polish. Imaging was performed using a Nikon Eclipse 80i epifluorescence microscope. The number of $pFAK^+$ vesicles was semi-quantified using CellProfiler image analysis software.[36] Briefly, green and blue channels were subtracted from the red channel images to reduce artifacts using the ImageMath module. Then, the number of $pFAK^+$ vesicles in each image was counted using the IdentifyPrimaryObject module, with a pixel size threshold set between 3 and 60.

2.10. Western Blot Analysis. To determine protein induction by CRT on NFs, Western blot analysis was employed. Briefly, HFFs were seeded onto NFs at a density of 5.7×10^3 cells/cm^2 and allowed to attach for 6−8 h and treated with appropriate medium (i.e., FBS-reduced complete medium with or without 100 ng/mL CRT) for 48 h, and cell lysates were prepared with 1× radioimmunoprecipitation assay lysis buffer (Sigma) containing 1× protease inhibitor cocktail on ice. The protein concentration of each sample was determined using a Micro-BCA protein assay kit, and 15 μg of each protein sample in Laemmli buffer containing 5% β-mercaptoethanol was loaded on a sodium dodecyl sulfate-polyacrylamide gel electrophoresis (10% acrylamide) and transferred onto a polyvinylidene fluoride membrane for immunoblotting. The blots were blocked in 5% of nonfat dry milk in tris-buffered saline with 0.1% Tween (TBST) for 1 h followed by overnight incubation in primary antibodies at 4 °C: mouse anti-human fibronectin (BD Biosciences, 1:1000) or mouse anti-integrin β1 (Santa Cruz Biotechnology, 1:500). To determine the levels of TGF-β1, the membrane was blocked overnight in 5% nonfat dry milk at 4 °C before incubating with the rabbit antibody[37] (2 μg/mL in 3% of nonfat milk in TBST) for 4 h at room temperature. β-actin (1:10,000 in 5% nonfat dry milk) was used as a loading control in all experiments. After incubation with primary antibodies, the membranes were washed thrice with TBST followed by addition of the secondary antibody for an incubation period of 1.5 h: goat anti-mouse (Invitrogen, 1:2000 in TBST in 5% nonfat dry milk) or goat anti-rabbit (Invitrogen, 1:2000 in TBST in 5% nonfat dry milk). The proteins transferred onto the membranes were detected using chemiluminescence-based SuperSignal West Femto Maximum Sensitivity Substrate (Invitrogen), and the image was captured using a ChemiDoc MP Imaging System (Bio-Rad). Densitometric scanning was performed using ImageJ, and the intensity of each band was normalized to β-actin. The data are expressed as fold change for each target protein in treatment groups over the PCX-0 control.

2.11. Statistical Analysis. All values are shown as average ± standard deviation. Statistical testing is described in the Results section; $p < 0.05$ was considered significant [$p < 0.05$ (*); $p < 0.01$ (**); and $p < 0.0001$ (****)], and $0.05 \leq p < 0.1$ was considered borderline significant (#).

3. RESULTS

3.1. Fabrication of CRT-Containing PCL/Col1 NFs. Following the established electrospinning conditions, CRT-containing PCL/Col1 NFs were fabricated. Successful incorporation of CRT into PCL/Col1 NFs was confirmed using attenuated total reflection-Fourier-transform infrared (ATR-FTIR), in which semi-quantification of signature absorption peaks showed a correlation with increasing concentrations of CRT (Supporting Information, Figure S1). SEM examination (Figure 1A) revealed a comparable fiber diameter (Supporting Information, Table S1) and organization despite addition and increasing concentrations of CRT at least up to PCC-100n conditions [322 ± 80 nm (PCX-0) vs 331 ± 80 nm (PCC-100n), $p = 0.57$ by a two-sided t-test assuming unequal variances]. However, at a 10-fold higher concentration (PCC-1μ), a noticeable change in fiber diameter was seen [$p < 1 \times 10^{-8}$ by single factor analysis of variance (ANOVA)],

https://doi.org/10.1021/acsami.2c13887
ACS Appl. Mater. Interfaces XXXX, XXX, XXX−XXX

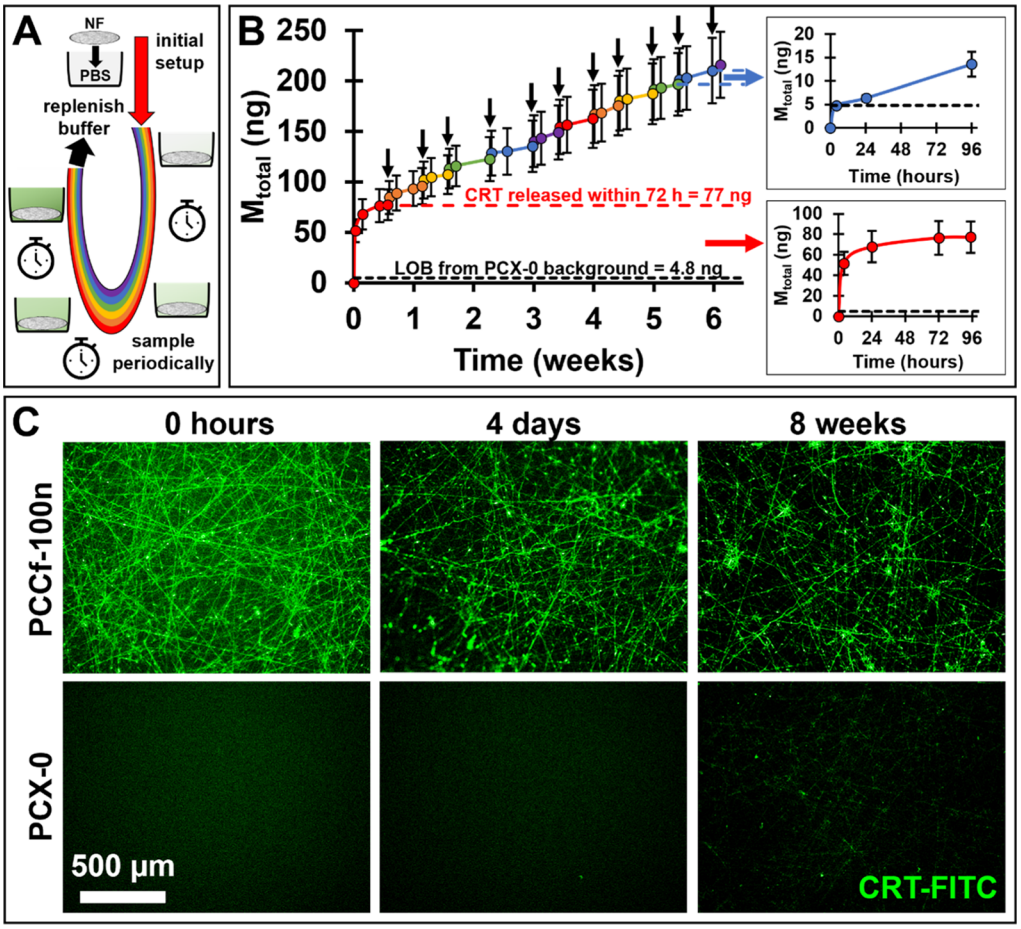

Figure 2. Sustained release of CRT out of CRT-containing NFs. (A) Schematic illustration of the experimental methodology used. (B) Cumulative mass of CRT-FITC released from PCCf-100n NFs on 15 mm-diameter glass coverslips over time. Color changes accompanied by black arrow heads indicate timepoints at which the receiver volume was fully replenished with fresh PBS. Insets: zoomed-in release graphs of the first and final round. (C) Green fluorescence images of PCCf-100n NFs and PCX-0 NFs submerged in PBS for different lengths of time. Green fluorescence above the background of corresponding PCX-0 images is CRT-FITC.

yielding smaller fibers with larger variability when using the same electrospinning parameters (Figure 1A). To better visualize CRT distribution in NFs, CRT-FITC was used to fabricate PCCf-100n NFs. As shown in Figure 1B, CRT-FITC was distributed uniformly throughout the NFs, suggesting that CRT was well dispersed in the electrospinning solution prior to the formation of NFs.

3.2. Sustained Release of CRT from CRT-Containing PCL/Col1 NFs. An initial release experiment was performed at 37 °C with shaking at 80 rpm to determine sufficient sampling timepoints to establish the release profile (Supporting Information, Figure S2). More appropriate release experiments were conducted at 37 °C under static conditions (i.e., without shaking) to better emulate the circumstances of in vitro cell culture and in vivo topical application. Within each round of the prolonged release study, samples were collected and replaced with PBS (70 μL) at 4 h, 24 h, and 48−120 h following complete removal and PBS replenishment (700 μL), with 2−5 day-long rounds repeating 11 times over a span of 6 weeks (Figure 2A,B). As noted, a significant amount of CRT-FITC was burst released within 4 h (52 ± 11 ng) followed by a slower release during the first round (red graph of the inset in Figure 2B), with 77 ± 16 ng of CRT-FITC released within the first 72 h and no further release observed thereafter (p = 0.19 by the paired t-test) until replenishment with fresh PBS (i.e., starting a new "round" of release). During every subsequent round, smaller amounts of CRT-FITC (9−19 ng) were released from the PCCf-100n NFs, with a total of 210 ± 32 ng released after 11 rounds of PBS replenishment. Importantly, the smaller amounts of CRT-FITC released during rounds 2−11 remained distinguishable above background levels, as demonstrated for "round 11" in the top inset (blue graph) of Figure 2B. To determine this background, PCX-0 NF samples were subjected to the same release experiment at the same time, and the baseline in all graphs of Figure 2B (4.8 ± 0.9 ng) represents the average false mass calculated from PCX-0 samples across all 11 rounds of the prolonged release study independently, akin to a limit of blank (LOB).[38] To visually confirm the CRT-FITC release, fluorescence images were taken with PCCf-100n NFs throughout the release experiment (Figure 2C). The fluorescence signal decreased in the PCCf-100n group yet remained clearly distinguishable even after 8 weeks. Interestingly, after 8 weeks submersion in PBS, very faint fluorescence was seen with PCX-0 NFs, most likely due to the autofluorescence of Col1.

3.3. Resistance to Proteolytic Degradation of CRT in CRT-Containing PCL/Col1 NFs. To determine whether CRT electrospun into NFs is putatively protected from proteolytic degradation compared with CRT without NFs (i.e., free CRT), elastase, subtilisin, cathepsin G, and proteinase K were

https://doi.org/10.1021/acsami.2c13887
ACS Appl. Mater. Interfaces XXXX, XXX, XXX−XXX

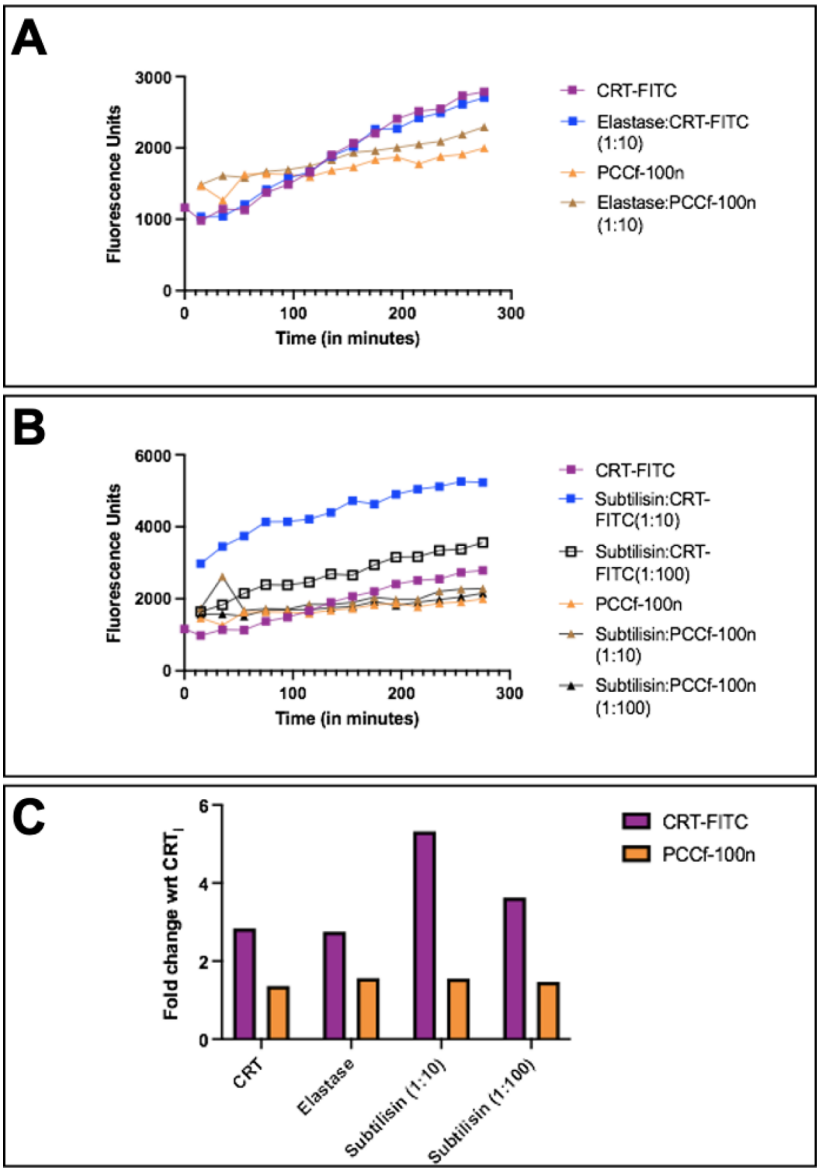

Figure 3. Proteolytic resistance of CRT-containing NFs. Effect of (A) elastase (at a molar ratio of 1:10) and (B) subtilisin (at a weight ratio of 1:10 and 1:100) on free CRT-FITC and PCCf-100n NFs submerged in PBS measured as fluorescence intensity of solution over time. (C) Fold change is presented as fluorescence after 275 min with or without the enzyme relative to fluorescence of CRT-FITC or PCCf-100n at 15 min without the enzyme (CRTi), respectively.

separately incubated with CRT-FITC or PCCf-100n NFs, and protein stability was assessed by measuring the fluorescence intensity of the solution or supernatant, respectively. As shown in Figure 3A, over a period of ~4.5 h, a similar incremental increase in fluorescence was observed for untreated free CRT-FITC compared to that in elastase-treated free CRT-FITC, both showing a 2.8-fold change in fluorescence units (Figure 3C). However, the relative increase in fluorescence intensity over time following elastase treatment was less for CRT-FITC sequestered in NFs at 1.6-fold compared to 1.4-fold. Treatment of CRT-FITC with subtilisin at a ratio of 1:10 and 1:100 (enzyme to protein) gave a dose-dependent increase in fluorescence intensity (Figure 3B) with a remarkable fold change of 5.3 at the 1:10 enzyme dilution and 3.6 at 1:100 (Figure 3C). Interestingly, as with elastase, there was a consistent unchanged fluorescence intensity in the PCCf-100n NFs in the presence or absence of subtilisin during the incubation period. PCCf-100n NFs treated with subtilisin at 1:10 and 1:100 ratios showed a fold change of 1.6 and 1.5, respectively (Figure 3C). Therefore, the data suggest that CRT sequestered in NFs (PCCf-100n) is well protected from proteolytic digestion within a 4.5 h digestion period by subtilisin, an enzyme that could be high in an infected wound. Moreover, within the NFs, even at a 10 times higher concentration of subtilisin, CRT was nearly equally stabilized. Furthermore, incubation of PCCf-100n and CRT-FITC separately with cathepsin G, another enzyme released by cells in the wound, and proteinase K, a proteolytic enzyme with broad substrate specificity, gave similar results such that CRT sequestered in the NFs (PCCf-100n) increased fewer relative fluorescence units over time upon enzyme exposure than an equal amount of CRT-FITC free in solution (Supporting Information, Figure S3).

3.4. Retention of Fibroblast Response to CRT in CRT-Containing PCL/Col1 NFs. To determine whether CRT incorporated into NFs retained its ability to stimulate cell

https://doi.org/10.1021/acsami.2c13887
ACS Appl. Mater. Interfaces XXXX, XXX, XXX−XXX

proliferation, a function important for increasing cell numbers in the wound,[11,12] HFFs seeded onto PCC NFs were assessed for their proliferative capacity compared to those cultured on PCX-0 NFs. Examination of the culture under phase-contrast imaging revealed a higher number of HFFs on PCC-100n NFs relative to PCX-0 NFs (Figure 4A). HFFs appeared well

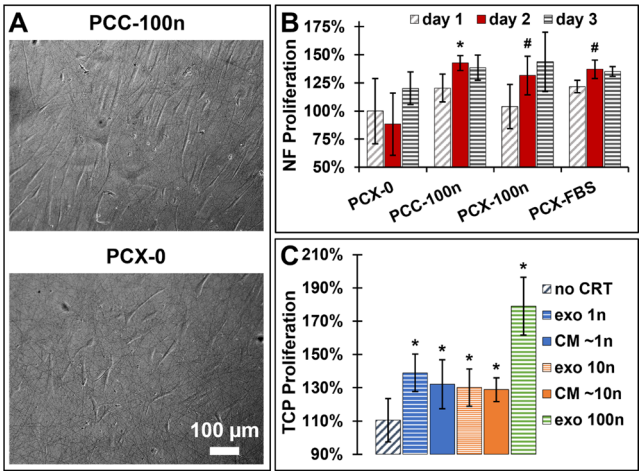

Figure 4. Proliferation of HFFs in response to various CRT conditions. (A) Phase contrast images of HFFs seeded at 5.2×10^3 cells/cm^2 on NFs containing CRT (PCC-100n) or without CRT (PCX-0) and cultured for 7 d. (B) Quantified proliferation of HFFs seeded at 5.7×10^3 cells/cm^2 on NFs and cultured over 3 d. NFs containing CRT (PCC-100n) were compared to NFs without CRT (PCX-0), with exogenous CRT (PCX-100n) and FBS (PCX-FBS) serving as controls. (C) Proliferation of HFFs in response to CRT released from NFs (conditioned medium: CM) and unprocessed CRT (exo) compared to that of control without CRT (no CRT). HFFs were seeded at 5.7×10^3 cells/cm^2 on TCP and then treated and cultured over 6 d. (B,C) * indicates $p < 0.05$, and # indicates $p < 0.10$ by means of unpaired *t*-tests assuming unequal variance compared to the control without CRT [PCX-0 in (B) or no CRT in (C)] at the same timepoint.

attached and spread on both PCC-100n and PCX-0 NFs. The observed increase in HFF proliferation was also verified using a resazurin assay (Figure 4B). No differences existed between all groups tested on day 1 ($p = 0.42$ by single-factor ANOVA), indicating that initial cell seeding was equal such that future timepoints could be directly compared to elucidate proliferation differences. Accordingly, statistically significant differences were identified between groups on day 2: the PCC-100n group (143 ± 7%) was significantly greater than the PCX-0 group (88 ± 28%) ($p = 0.04$ by the one-sided *t*-test assuming unequal variances), and borderline significance was found when comparing the PCX-100n (132 ± 17%) and PCX-FBS (137 ± 8%) groups to the PCX-0 group ($0.05 < p < 0.053$ by one-sided *t*-tests assuming unequal variances). Interestingly, no statistical differences existed again between all groups on day 3 ($p = 0.38$ by single-factor ANOVA), suggesting that the cells had reached confluency with no further space available to observe proliferation. Confluency of the cell cultures was confirmed by subsequent immunofluorescence staining (data not shown).

To demonstrate whether the CRT released from NFs exhibits a similar bioactivity to the unprocessed CRT (i.e., not electrospun into NFs and therefore without exposure to the organic solvent and electric field), HFFs cultured on TCP were incubated with either CM containing NF-released CRT or medium containing unprocessed CRT. Upon confirmation of the comparable cell number in each well (Supporting Information, Figure S4, $p = 0.97$ by single-factor ANOVA), the cells were subsequently cultured with the different media for a total of 6 days. As shown in Figure 4C, the normalized proliferation of the negative control ("no CRT") and positive control ("exo 100n") was 111 ± 13% and 179 ± 17%, respectively, and groups with either CM or exo showed values between these controls: 139 ± 11% for "exo 1n", 132 ± 15% for "CM ~ 1n", 130 ± 11% for "exo 10n", and 129 ± 7% for "CM ~ 10n". Therefore, the presence of CRT in the culture medium, whether unprocessed (exo) or released from NFs (CM), similarly promoted cell proliferation compared to the cultures receiving medium without CRT ($p < 0.05$ by one-sided t-tests assuming unequal variances).

Another biological function important for wound healing is the migration of fibroblasts into the wound for granulation tissue formation. Previous studies have shown that free CRT could induce chemotaxis and motility of fibroblasts.[11,12,14] To determine whether CRT electrospun into NFs retained the ability to mediate migration, HFFs seeded onto PCC compared to those seeded on PCX-0 NFs were examined for cumulative motogenic behavior using in vitro wound-gap closure assays and for single-cell directional and velocity migration using time-lapse imaging in a motility assay. In an initial experiment in which proliferation was not blocked, the PCC-100n NFs appeared to promote greater wound-gap closure compared to the PCX-0 control after 51 h (Figure 5A). To more accurately quantify gap closure and exclude the contribution of cell proliferation, cells were fluorescently labeled with DiD prior to seeding and then pretreated with mitomycin C after adhesion. Through time-lapse fluorescence imaging, periodic gap closure was readily quantified (Figure

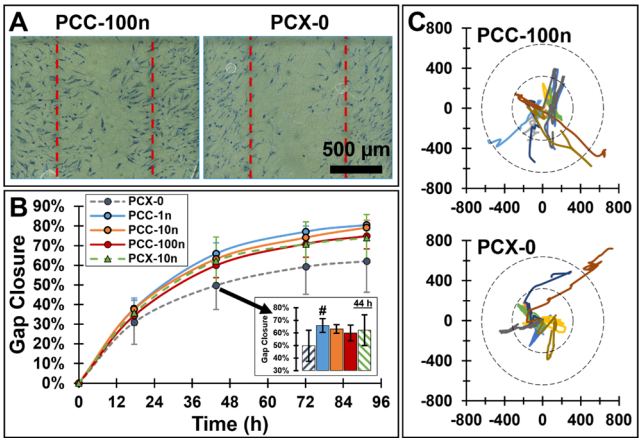

Figure 5. Motogenic behavior of HFFs on CRT-containing NFs. (A,B) Migration of HFFs on CRT-containing NFs using wound-gap closure assays. (A) Brightfield images of methylene-blue-stained HFFs allowed to migrate and proliferate on NFs for 51 h. The initial gap is approximated in red. (B) Quantified continuous gap closure of HFFs allowed to migrate on NFs over 91 h. Inset: 44 h timepoint. # indicates $p < 0.10$ by means of the unpaired *t*-test assuming unequal variances compared to that of the control without CRT (PCX-0) at the same timepoint. (C) Motility of HFFs on CRT-containing NFs. Migration paths of 10 individual cells on NFs containing CRT (PCC-100n) or without CRT (PCX-0) over a minimum of 4 h. Circles represent 320 and 640 μm distance marks.

https://doi.org/10.1021/acsami.2c13887
ACS Appl. Mater. Interfaces XXXX, XXX, XXX−XXX

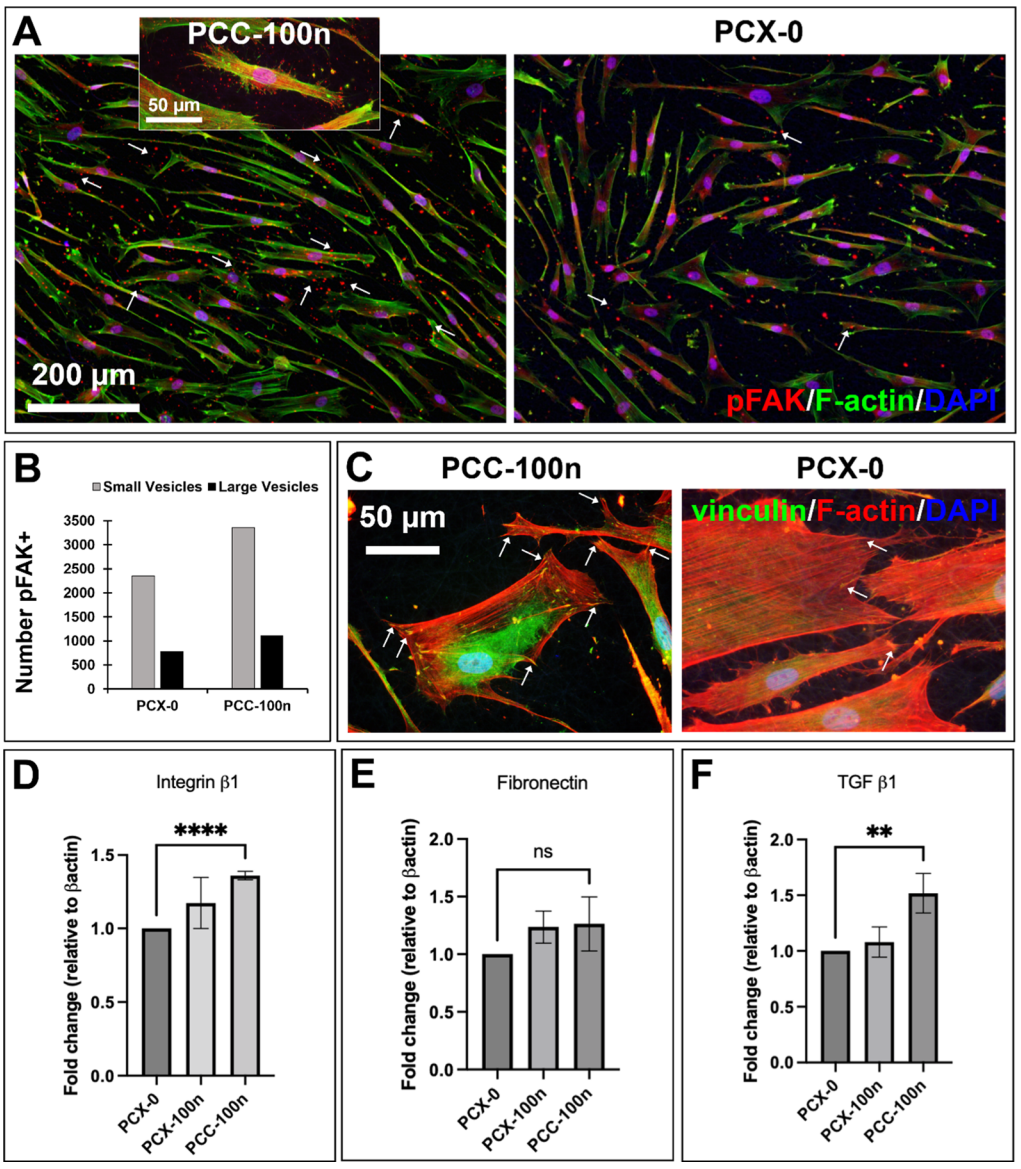

Figure 6. Protein expression of HFFs on CRT-containing NFs. (A,C) HFFs immunofluorescent-stained for (A) pFAK (red), F-actin fibers (green), and cell nuclei (blue) or (C) vinculin (green), F-actin fibers (red), and cell nuclei (blue) after 24 h culture on NFs containing CRT (PCC-100n) or without CRT (PCX-0). White arrows indicate (A) $pFAK^+$ vesicles or (C) $vinculin^+$ focal adhesions. Inset in (A): higher magnification of a single cell showing $pFAK^+$ vesicles being secreted. (B) Quantification of the number of $pFAK^+$ vesicles found in (A) segregated by size. (D–F) Western blot analysis of HFFs after 48 h culture on CRT-containing NFs (PCC-100n) or corresponding controls (PCX-100n and PCX-0). Densitometric analysis of (D) integrin $\beta 1$, (E) fibronectin, and (F) TGF-$\beta 1$ using β-actin as a control. Fold change was calculated over PCX-0. ** indicates $p < 0.01$, and **** indicates $p < 0.0001$ by means of unpaired t-tests compared to those of the control without CRT (PCX-0).

5B). No statistical difference in gap closure was found between groups with or without CRT, particularly at the earliest timepoint (i.e., at 18 h: $p = 0.67$ by single-factor ANOVA). However, at later timepoints, there did appear to be a trend that the presence of CRT either in NFs or exogenously supplied slightly increased cell migration, and a borderline significance was seen between PCC-1n and PCX-0 groups ($0.05 < p < 0.10$ by one-sided t-tests assuming unequal variances at 44, 72, and 91 h). It is notable that the untreated control consistently showed a large standard deviation in individual experiments. The inset of Figure 5B highlights the gap closure of different groups at 44 h, wherein PCC-1n was 66 ± 6% compared to 50 ± 12% for PCX-0, and the other groups were 63 ± 3% (PCC-10n), 60 ± 6% (PCC-100n), and 62 ± 12% (PCX-10n). In terms of single cell motility, time-lapse observation showed that HFFs on PCC-100n NFs were more motile than those on PCX-0 NFs (Figure 5C).

To further characterize the migratory phenotype supported by CRT electrospun into NFs, immunofluorescent staining for pFAK, vinculin, and F-actin was performed for HFFs cultured on PCX-0 and PCC-100n NFs for 24 h. As shown in Figure 6A, pFAK (red fluorescence) was predominantly distributed in the perinuclear region of HFFs cultured on PCX-0 NFs, whereas a higher expression of pFAK was localized at the cell peripheries and, remarkably, in extracellular vesicles left behind by the cells (Figure 6A, inset) on PCC-100n NFs. This trail of extracellular vesicles was also observed in the brightfield images of an HFF culture on PCC-10n NFs (Supporting Information, Figure S5). Semi-quantification of the pFAK-enriched vesicles (red fluorescence) showed that a greater amount was present

https://doi.org/10.1021/acsami.2c13887
ACS Appl. Mater. Interfaces XXXX, XXX, XXX−XXX

in the PCC-100n group (Figure 6B). Although HFFs on both types of NFs were spread with an elongated morphology, cells on PCC-100n NFs appeared more uniformly stretched with more lamellipodia and filipodia than those on PCX-0 NFs (Figure 6A). Typical vinculin (green fluorescence)-capping F-actin fibers (red fluorescence) were seen in HFFs cultured on both types of NFs but were much more pronounced on PCC-100n NFs (Figure 6C, arrows). Although evenly distributed F-actin fibers were seen across HFFs cultured on PCX-0 NFs, F-actin fibers were mainly located in the peripheral region of cells on PCC-100n NFs, suggesting a migratory cell phenotype.

Additionally, to determine whether CRT electrospun into NFs retained the ability to induce ECM proteins and integrin β1,[14] HFFs were cultured on NFs containing CRT (PCC-100n), NFs without CRT (PCX-0), or NFs without CRT but with CRT supplied exogenously as a control (PCX-100n) and compared for levels of integrin β1, fibronectin, and TGF-β1 (a key inducer of ECM proteins). The level of fibronectin was shown to be induced in HFFs seeded on both PCX-100n and PCC-100n NFs (Figure 6E, Supporting Information, Figure S6). However, the difference was not statistically significant as compared to that of PCX-0. HFFs seeded on PCC-100n and PCX-100n NFs showed an increased expression of integrin β1, which was significant at 1.4-fold higher than that of cells cultured on PCX-0 (Figure 6D, Supporting Information, Figure S6). HFFs seeded on PCC-100n showed a statistically significant induction of TGF-β1 as well marked by the ~1.4-fold change as compared to those of both PCX-0 and PCX-100n groups as shown in Figure 6F and Supporting Information, Figure S6.

3.5. Retention of Keratinocyte Response to CRT in CRT-Containing PCL/Col1 NFs. Similar to that of HFFs, proliferation of HEKs on various NFs was assessed by resazurin assay. As shown in Figure 7A, no significant difference in cell proliferation (p = 0.40 by single-factor ANOVA) were seen on day 1 among PCX-0, PCC-100p, and PCX-100p groups. However, after culture for 3 days, proliferation on PCC-100p NFs was significantly greater than that on PCX-0 NFs (1266 ± 145% vs 852 ± 193%, p = 0.02 by the one-sided t-test assuming unequal variances). Fascinatingly, this was not true when the PCX-100p group, in which CRT was added exogenously, was compared to the PCX-0 group (817 ± 187% vs 852 ± 193%, p = 0.41 by the one-sided t-test assuming unequal variances). By day 5, the normalized metabolic activity was decreased for all the groups (PCX-0, PCC-100p, and PCX-100p reaching 393 ± 61%, 524 ± 39%, and 423 ± 32%, respectively) despite the statistical difference between the PCC-100p and PCX-0 groups (p = 0.03 by the one-sided t-test assuming unequal variances). Cell detachment was observed in all groups, likely accounting for this decrease, which could have been caused by the long incubation with resazurin.[39] Notably, live/dead staining showed negligible cell death (data not shown). To further confirm the promotion of HEK proliferation by PCC-100p NFs, immunofluorescent staining for Ki67 was performed immediately after the resazurin assay. Apparently, substantially more Ki67-positive cells (green fluorescence) were found on the PCC-100p NFs than on the PCX-0 NFs (Figure 7B). Staining for F-actin and nuclei (DAPI) did confirm more cells on PCC-100p NFs than on PCX-0 NFs (Figure 7C).

As CRT was shown to stimulate migration of keratinocytes accounting for the rapid reepithelialization in vivo,[11] the retention for CRT electrospun into NFs to induce HEK

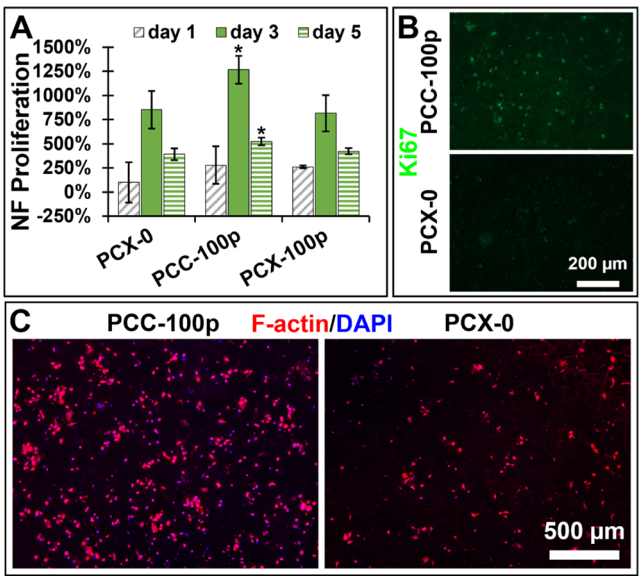

Figure 7. Proliferation of HEKs on CRT-containing NFs. (A) Quantified proliferation of HEKs seeded at 1.0 × 10^4 cells/cm^2 on NFs and cultured over 5 d. NFs containing CRT (PCC-100p) were compared to NFs without CRT (PCX-0), with exogenous CRT (PCX-100p) serving as a control; * indicates $p < 0.05$ by means of unpaired t-tests assuming unequal variances compared to the control without CRT (PCX-0) at the same timepoint. (B) HEKs immunofluorescently stained for Ki67 (green) after 5 day culture on NFs containing CRT (PCC-100p) or without CRT (PCX-0). (C) HEKs immunofluorescently stained for F-actin fibers (red) and cell nuclei (blue) after 8 d culture on NFs containing CRT (PCC-100p) or without CRT (PCX-0).

migration was evaluated using wound-gap closure assays and immunostaining for selected markers. Figure 8A displays the quantified results of a wound healing gap closure assay in which HEKs were labeled with DiD and pretreated with mitomycin C. After 6 h, only HEKs on PCC-100p NFs showed significantly higher gap closure than those on PCX-0 NFs (p = 0.05 by the one-sided t-test assuming unequal variances). Throughout the course of the experiment, percent gap closure progressively increased in all groups, though it appeared to level off in the PCX-0 group at approximately 36 h. At the final timepoint examined (60 h, Figure 8B), the presence of CRT—both incorporated in NFs (PCC groups) or supplemented exogenously into the medium (PCX-10p group)—significantly promoted gap closure via cell migration relative to the PCX-0 control. A borderline significance (p = 0.08 by the one-sided t-test assuming unequal variances) was seen between the PCC-1p and PCX-0 groups at this timepoint, but all other PCC groups were statistically significant at $p < 0.05$. The calculated gap closure at 60 h was 29 ± 2% for PCX-0, 39 ± 7% for PCC-1p, 50 ± 8% for PCC-100p, 47 ± 7% for PCC-10n, and 41 ± 6% for PCX-10p. Immunofluorescent staining of samples previously used in the proliferation study revealed a higher extracellular deposition of laminin-5 (red fluorescence) in the PCC-100p group than that in the PCX-0 group (Figure 8C). Notably, HEKs grown on PCC-100p NFs were also generally larger and more elongated than those on PCX-0 NFs (Figures 7C and 8C). These findings suggest a migratory phenotype consistent with the bioactivity of PCC-100p NFs shown in Figure 8A,B.

https://doi.org/10.1021/acsami.2c13887
ACS Appl. Mater. Interfaces XXXX, XXX, XXX−XXX

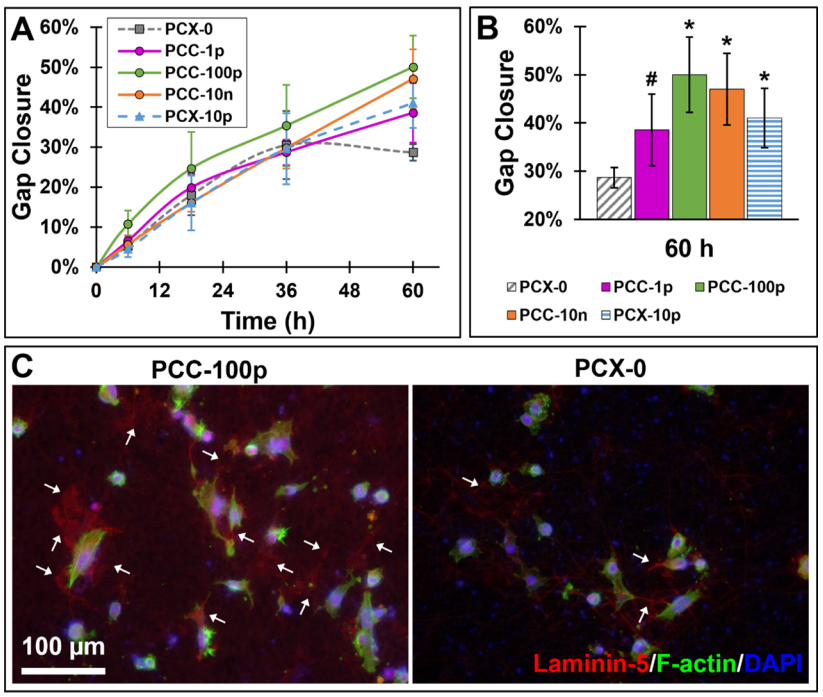

Figure 8. Migration of HEKs on CRT-containing NFs. (A) Quantified continuous gap closure of HEKs allowed to migrate on NFs over 60 h in a wound-gap closure assay. (B) Zoom in on the 60 h timepoint from (A). * indicates $p < 0.05$, and # indicates $p < 0.10$ by means of unpaired t-tests assuming unequal variances compared to those of the control without CRT (PCX-0) at the same timepoint. (C) HEKs immunofluorescently stained for laminin-5 (red, white arrows), F-actin fibers (green), and cell nuclei (blue) after 5 day culture from an initial seeding density of 1.0×10^4 cells/cm^2 on NFs containing CRT (PCC-100p) or without CRT (PCX-0).

4. DISCUSSION

It is well documented that cells are sensitive to stimulation by topography of their residing microenvironment.[40] Therefore, possible topographical effects (such as through differing fiber morphologies) needed to be ruled out for the cell studies of CRT effects (presence vs absence) herein. PCX-0 and PCC-100n NFs were comparable in terms of fiber uniformity and fiber diameter. As CRT is negatively charged,[41] the degenerated fiber morphology seen in the PCC-1μ NF group is likely due to the high CRT content altering the conductivity of the polymer solution beyond a certain threshold, thereby changing the electrospinnability.[42,43] Even at this high CRT concentration, NFs comparable to the PCX-0 and PCC-100n groups could still be obtained, for example, by increasing the polymer concentration as previously shown.[44] Since fibroblasts were previously demonstrated to be sensitive to exogenously provided CRT at ng/mL levels[11,12] and keratinocytes at pg/mL levels,[11] the need for a higher concentration of CRT within the NFs did not appear to be warranted. Therefore, due to the apparent morphological similarities, PCX NFs and PCC NFs containing CRT at PCC-100n concentrations and below (outlined in Table 1) were used in these studies.

The concentration gradient was expected to be the main driving force affecting the release of CRT from NFs through simple diffusion, considering that PCL, the main component of the NFs, is a slow-eroding, hydrophobic polymer.[45] Accordingly, in the prolonged release experiment, the full receiver volume was replenished with fresh PBS every 2−5 days to mimic cell culture medium changes. This is consistent with the in vivo situation wherein the CRT concentration gradient would be reduced by diffusion out of the immediate wound area, adsorption to the surrounding ECM, and/or uptake by cells. In this way, release of CRT-FITC from PCCf-100n NFs was confirmed to be concentration-dependent since the complete replenishment of the receiver volume resulted in a short burst release period of about 4 h at each round (even when the previous round had leveled off release), followed by a period of more steady release over the course of 2−5 days. Notably, the burst release is a result of the simple blend method used in this proof-of-concept study and could be reduced in future studies by various means, as reviewed by Chou et al.[46] Fluorescent imaging conducted throughout the release experiment corroborated the finding that CRT-FITC release was to a certain degree sustained over the course of at least 6 weeks since green fluorescence attributed to CRT-FITC was still seen throughout the PCCf-100n NFs after 8 weeks submersion in PBS.

The wound environment contains abundant enzymes released by cells that are important in the process of healing a wound and derived from commensal and pathogenic bacteria. Although proteases are key players in wound debridement necessary for normal healing,[47] the abundant presence of proteases is a notable feature of chronic wounds, greatly contributing to their tissue damage and chronicity.[48] As such, the chronic wound proteolytic environment can degrade and inactivate therapeutic biological molecules rendering their topical application ineffective. One of the goals of this study was to demonstrate whether CRT incorporated into NFs by means of electrospinning would protect the molecule from proteolytic degradation. Fluorescence intensity of CRT-FITC in PBS contributed by PCCf-100n NFs compared to that of free CRT-FITC was used as an estimate of CRT stability afforded by NF protection. Notably, CRT appears not to be degraded by cathepsin G or elastase (two abundant enzymes in wound fluid) since fluorescence intensity remained unchanged for free CRT-FITC (i.e., without NFs). Importantly, the results

https://doi.org/10.1021/acsami.2c13887
ACS Appl. Mater. Interfaces XXXX, XXX, XXX−XXX

suggest that in comparison to free CRT-FITC in solution, CRT in NFs (PCCf-100n) was protected from proteolysis by subtilisin, a bacterial enzyme, and proteinase K, a potent broad substrate specific enzyme. Whether the increase in fluorescence intensity upon incubation with these enzymes reflects the generation of proteolytic fragments or a conformational change in CRT exposing FITC-labeled amines is not known.

A highly cellular granulation tissue with abundant collagen and other ECM proteins is critical for reconstruction of the wound defect. Fibroblasts are the most prominent cells of the dermis which migrate into the wound, proliferate and produce granulation tissue,[49] providing a substrate for keratinocytes to migrate from the wound edge for reepithelialization. Previous studies have demonstrated that CRT functions as a chemoattractant to recruit fibroblasts to reconstruct the wound, stimulates proliferation, upregulates α-smooth muscle actin (for wound contraction) and integrins, and induces ECM proteins.[11,12,14,50] Importantly, CRT incorporated into NFs retained its biological activities of inducing proliferation (Figure 4), migration (Figure 5), and ECM protein and integrin expression (Figure 6) by HFFs.

The increased mitogenic response of HFFs compared to that of PCX-0 (no CRT) was similar for PCC-100n (CRT electrospun into NFs) and PCX-100n (PCX plus 100 ng/mL exogenous CRT). Thus, the increased proliferation observed in the PCC-100n and PCX-100n groups on day 2 indicates that the mitogenic activity of CRT was retained during its processing into NFs. Furthermore, the CRT released from the NFs, as CM, stimulated proliferation of HFFs grown on TCP in a comparable manner to the intact (unprocessed) CRT. Although CRT induced a statistically significant proliferative response in these NF experiments, the induction of HFF migration on NFs by CRT as measured by the gap closure rate was not statistically significant. Significance appeared not to be attained because the PCX-0 group showed a high standard deviation, which might be related to random motility of individual cells on NFs. In contrast, HFFs cultured on PCC-100n NFs showed little variation in the motility assay (Figure 5C). Despite the lack of statistical significance, there was nonetheless a trend of CRT increasing the rate of gap closure observed at timepoints after 18 h, which was of borderline significance in the PCC-1n group. As the peak response of HFF migration in a scratch assay on TCP was previously reported to occur at 1 ng/mL CRT with decreased activity obtained at higher concentrations,[11] it partially makes sense that borderline significance was only found with the PCC-1n NFs in this experiment since with higher CRT concentrations, the migratory response may diminish. Nonetheless and importantly, these migration experiments were performed in the presence of mitomycin C to block proliferation. Clearly, the gap closure of HFFs on CRT-NFs was wholly related to motogenicity.

Many cell adhesion complexes have been shown to elicit mechanosensing effects, and vinculin is a particularly well characterized focal adhesion protein that links transmembrane adhesion receptors such as integrins to cytoskeletal components such as F-actin fibers to form adhesion complexes.[51] Although there was no apparent distinction between induction of migration for gap closure of HFFs by CRT on NFs, related to adhesion and migration, more prevalent vinculin staining was observed in HFFs cultured on PCC-100n NFs than in those cultured on PCX-0 NFs, suggesting the formation of more mature cell adhesion complexes at cell-NF contacts. Previous work has uncovered a relationship between vinculin (i.e., focal adhesion complex) size and cell migration speed,[52] suggesting that HFFs on PCC-100n NFs may be more motile, which agrees with the observations in Figure 5C. In addition to vinculin, the F-actin staining stretched across the cells suggests a more motile phenotype, and the stretched morphology with lamellipodia and filopodia observed in Figure 6A,C evidently supports cell motogenicity, as widely established.[53] Similar to vinculin, FAK, a cytoplasmic protein tyrosine kinase, is associated with mechanosignaling.[54] Notably, the increased lamellipodium protrusion, which is associated with Rac-dependent functions, and the pFAK staining observed for HFFs on PCC-100n NFs are consistent with cell adhesion and the migratory phenotype.[55] Interestingly, another unique observation of HFFs cultured on PCC-100n NFs was the trail of pFAK-positive extracellular vesicles released by the cells. Based on the size, these vesicles implicate a migration-specific exosome recently identified as migrasomes.[56]

Previously, CRT was shown to induce ECM proteins and TGF-β1 by fibroblasts in vitro.[14] Furthermore, CRT could induce ECM proteins via TGF-β1 Smad2/3 signaling, which was modulated by CRT ostensibly to ameliorate scarring.[57] In addition, both α5 and β1 integrins were induced by CRT. The studies herein demonstrate that HFFs seeded on CRT-NFs showed a comparable increase in integrin β1 in response to CRT for both NFs electrospun with CRT and NFs with CRT added exogenously. Therefore, in addition to the ability of CRT to promote cell motility and proliferation upon incorporation into NFs, the induction of integrin β1, an important receptor for cell migration,[58] and the presence of fibronectin, an important component of granulation tissue and collagen organization,[59] were also retained, consistent with known CRT bioactivities. A mechanism for CRT-induced migration of HFFs might be related to the upregulation of fibronectin as a substrate for integrin $\alpha5\beta1$ signaling. It is interesting to note that high levels of TGF-β1 were detected on HFFs cultured on PCC-100n NFs, and since CRT modulates TGF-β1 to favor tissue regeneration, this suggests that CRT in PCC-100n NFs could have the same effect in vivo.

Similar to previous findings in both in vitro and in vivo porcine and diabetic mouse wound experiments,[11,12] CRT electrospun into NFs was able to retain its inductive functions to promote proliferative and migratory responses of HEKs. Distinct from the results obtained with HFFs, in which CRT electrospun into NFs (PCC-100n) or added exogenously to NFs (PCX-100n) exhibited similar support to cell proliferation, there was statistically significant increase in HEK proliferation only on CRT-NFs and not when cells were exposed to exogenously added CRT. A possible explanation of such might be based on the timing of the release of CRT from the NFs in comparison to adding exogenous CRT. As such, HEKs are exposed to CRT within the NFs immediately upon seeding in the PCC-100p group, rather than adhesion to NFs prior to exogenously supplying CRT to the cells on NFs in the PCX-100p group. Accordingly, certain cellular effects may be elicited even prior to their attachment by the burst-released CRT from the CRT-NFs. Regardless, subsequent immunostaining with Ki67 of the HEKs supported the differences obtained between NFs with and without CRT. With respect to induction of HEK migration by CRT-NFs, while HEKs showed a greater response to CRT electrospun into NFs (e.g., PCC-100p vs PCX-0), exogenously added CRT to HEKs on NFs (PCX-10p; used as the 10 pg/mL exogenous

https://doi.org/10.1021/acsami.2c13887
ACS Appl. Mater. Interfaces XXXX, XXX, XXX−XXX

control[11]) also supported a migratory response of these cells. Moreover, consistent with migration, an increase in laminin-5[60] was observed in extracellular deposits near the migrating cells.

5. CONCLUSIONS

In this study, CRT, a biological molecule that was previously shown to be effective topically in animal wound healing models,[11,12] was incorporated into PCL/Col1-based electrospun NFs as a biomimetic ECM, with the idea that this hybrid scaffold might (1) retain the biological activity of CRT while sustaining its release and protecting it against degradation by enzymes in a chronic wound bed and (2) provide synergism of biological and mechanical cues to further promote wound healing functions of cells. Although this study provides proof of concept for the potential of CRT-NFs to be developed as a new therapeutic modality for both acute and chronic wounds, future studies are needed to select an ideal scaffold formulation to proceed with studies for clinical translation. Important considerations in this process would include fiber diameter (e.g., a smaller diameter may be more favorable for keratinocyte migration[19]), polymeric matrix composition (e.g., polymers with different degradation properties could alter the release of CRT), optimal dosage of CRT and also, for consideration, different layers of NF scaffolds supporting various cell types and functions for cutaneous tissue regeneration.

■ ASSOCIATED CONTENT

Supporting Information

The Supporting Information is available free of charge at https://pubs.acs.org/doi/10.1021/acsami.2c13887.

Fiber diameters measured from SEM images, ATR-FTIR spectra of NFs, initial release experiment to determine relevant timepoints, further proteolytic studies with cathepsin G and proteinase K, day 2 results, exosomes from HFFs on PCC-10n NFs, and immunoblots (PDF)

■ AUTHOR INFORMATION

Corresponding Authors

Leslie I. Gold − *Departments of Medicine and Pathology, New York University School of Medicine, New York, New York 10016, United States*; Phone: +1 (212)-263-6320; Email: Leslie.Gold@nyulangone.org

Hongjun Wang − *Department of Biomedical Engineering, Stevens Institute of Technology, Hoboken, New Jersey 07030, United States; Department of Chemistry and Chemical Biology and Center for Healthcare Innovation, Stevens Institute of Technology, Hoboken, New Jersey 07030, United States;* orcid.org/0000-0003-3455-8523; Phone: +1 (201)-216-5556; Email: Hongjun.Wang@stevens.edu

Authors

Mary E. Stack − *Department of Biomedical Engineering, Stevens Institute of Technology, Hoboken, New Jersey 07030, United States*

Sarita Mishra − *Departments of Medicine and Pathology, New York University School of Medicine, New York, New York 10016, United States*

Matangi Parimala Chelvi Ratnamani − *Department of Biomedical Engineering, Stevens Institute of Technology, Hoboken, New Jersey 07030, United States*

Haoyu Wang − *Department of Biomedical Engineering, Stevens Institute of Technology, Hoboken, New Jersey 07030, United States*

Complete contact information is available at: https://pubs.acs.org/10.1021/acsami.2c13887

Author Contributions

M.S., S.M., L.G., and H.W. wrote the manuscript. M.S. prepared samples for all studies and performed SEM imaging and release experiments. H.W. performed ATR-FTIR. S.M. performed enzyme studies. M.S. and S.M. performed HFF culture. M.S. performed proliferation and wound-gap closure analyses. M.S., H.W., and M.P.R. performed HFF immunostaining and imaging. M.P.R. performed HFF motility and pFAK analyses. S.M. performed Western blot. M.S. performed all HEK experiments. All authors have given approval to the final version of the manuscript.

Funding

Financial support for this work was provided by the NIDDK Diabetic Complications Consortium (RRID: SCR_001415, www.diacomp.org), grants DK076169 and DK115255.

Notes

The authors declare no competing financial interest.

■ ACKNOWLEDGMENTS

The authors are grateful for the financial support provided to L.I.G. by the NIDDK Diabetic Complications Consortium (RRID: SCR_001415, www.diacomp.org), grants DK076169 and DK115255. The authors would also like to thank Dr. Tsengming (Alex) Chou for use of the facilities in the Laboratory for Multiscale Imaging at Stevens Institute of Technology and Dr. Jingyu Sun for her assistance with additional ATR-FTIR experimentation.

■ ABBREVIATIONS

CRT, calreticulin
PCL, polycaprolactone
Col1, collagen type I
NF, nanofiber
PCX NF, PCL/Col1 NF
PCC NF, PCL/Col1/CRT NF
FITC, fluorescein isothiocyanate isomer I
CRT-FITC, FITC-labeled CRT
PCCf NF, PCL/Col1/CRT-FITC NF
HFIP, 1,1,1,3,3,3-hexafluoro-2-propanol
TC, Tris-Ca buffer
PBS, phosphate buffered saline
MEM, Minimum Essential Medium
FBS, fetal bovine serum
KSF, keratinocyte serum-free medium
BPE, bovine pituitary extract
EGF, epidermal growth factor
KBM, keratinocyte basal medium
BPEI, branched polyethylenimine
DMSO, dimethyl sulfoxide
BSA, bovine serum albumin
FAK, focal adhesion kinase
pFAK, phosphorylated FAK
TGF-β1, transforming growth factor-β1
ECM, extracellular matrix
LOB, limit of blank
SEM, scanning electron microscopy

https://doi.org/10.1021/acsami.2c13887
ACS Appl. Mater. Interfaces XXXX, XXX, XXX−XXX

ATR-FTIR, attenuated total reflection-Fourier-transform infrared spectroscopy
DFU, diabetic foot ulcer
CTP, cellular and tissue-based product
DDS, drug delivery system
HFFs, primary human neonatal foreskin fibroblasts
HEKs, telomerase-immortalized human keratinocytes
ANOVA, analysis of variance
TCP, tissue culture plastic
CM, conditioned medium

REFERENCES

(1) Brem, H.; Stojadinovic, O.; Diegelmann, R. F.; Entero, H.; Lee, B.; Pastar, I.; Golinko, M.; Rosenberg, H.; Tomic-Canic, M. Molecular Markers in Patients with Chronic Wounds to Guide Surgical Debridement. *Mol. Med.* **2007**, *13*, 30−39.
(2) Armstrong, D. G.; Boulton, A. J. M.; Bus, S. A. Diabetic Foot Ulcers and Their Recurrence. *N. Engl. J. Med.* **2017**, *376*, 2367−2375.
(3) Boulton, A. J. M.; Vileikyte, L.; Ragnarson-Tennvall, G.; Apelqvist, J. The Global Burden of Diabetic Foot Disease. *Lancet* **2005**, *366*, 1719−1724.
(4) Jupiter, D. C.; Thorud, J. C.; Buckley, C. J.; Shibuya, N. The Impact of Foot Ulceration and Amputation on Mortality in Diabetic Patients. I: From Ulceration to Death, a Systematic Review. *Int. Wound J.* **2015**, *13*, 892−903.
(5) Margolis, D. J.; Bartus, C.; Hoffstad, O.; Malay, S.; Berlin, J. A. Effectiveness of Recombinant Human Platelet-Derived Growth Factor for the Treatment of Diabetic Neuropathic Foot Ulcers. *Wound Repair Regen.* **2005**, *13*, 531−536.
(6) Park, S. A.; Raghunathan, V. K.; Shah, N. M.; Teixeira, L.; Motta, M. J.; Covert, J.; Dubielzig, R.; Schurr, M.; Isseroff, R. R.; Abbott, N. L.; McAnulty, J.; Murphy, C. J. PDGF-BB Does Not Accelerate Healing in Diabetic Mice with Splinted Skin Wounds. *PLoS One* **2014**, *9*, No. e104447.
(7) Papanas, D.; Maltezos, E. Benefit-Risk Assessment of Becaplermin in the Treatment of Diabetic Foot Ulcers. *Drug Saf.* **2010**, *33*, 455−461.
(8) Walters, J.; Cazzell, S.; Pham, H.; Vayser, D.; Reyzelman, A. Healing Rates in a Multicenter Assessment of a Sterile, Room Temperature, Acellular Dermal Matrix Versus Conventional Care Wound Management and an Active Comparator in the Treatment of Full-Thickness Diabetic Foot Ulcers. *ePlasty* **2016**, *16*, No. e10.
(9) Marston, W. A.; Hanft, J.; Norwood, P.; Pollak, R. The Efficacy and Safety of Dermagraft in Improving the Healing of Chronic Diabetic Foot Ulcers. *Diabetes Care* **2003**, *26*, 1701−1705.
(10) Driver, V. R.; Lavery, L. A.; Reyzelman, A. M.; Dutra, T. G.; Dove, C. R.; Kotsis, S. V.; Kim, H. M.; Chung, K. C. A Clinical Trial of Integra Template for Diabetic Foot Ulcer Treatment. *Wound Repair Regen.* **2015**, *23*, 891−900.
(11) Nanney, L. B.; Woodrell, C. D.; Greives, M. R.; Cardwell, N. L.; Pollins, A. C.; Bancroft, T. A.; Chesser, A.; Michalak, M.; Rahman, M.; Siebert, J. W.; Gold, L. I. Calreticulin Enhances Porcine Wound Repair by Diverse Biological Effects. *Am. J. Pathol.* **2008**, *173*, 610−630.
(12) Greives, M. R.; Samra, F.; Pavlides, S. C.; Blechman, K. M.; Naylor, S.-M.; Woodrell, C. D.; Cadacio, C.; Levine, J. P.; Bancroft, T. A.; Michalak, M.; Warren, S. M.; Gold, L. I. Exogenous Calreticulin Improves Diabetic Wound Healing. *Wound Repair Regen.* **2012**, *20*, 715−730.
(13) Gold, L. I.; Pavlides, S.; Ojeda, J.; Eaton, B.; Panchal, R. A New Role for the Multifunctional Wound Healing Agent Calreticulin (CRT) in Combating Infection: Significance for Treating Diabetic Foot Ulcers. *Wound Repair Regen.* **2014**, *22*, A42.
(14) Pandya, U. M.; Manzanares, M. A.; Tellechea, A.; Egbuta, C.; Daubriac, J.; Jimenez-Jaramillo, C.; Samra, F.; Fredston-Hermann, A.; Saadipour, K.; Gold, L. I. Calreticulin Exploits TGF-β for Extracellular Matrix Induction Engineering a Tissue Regenerative Process. *FASEB J.* **2020**, *34*, 15849−15874.
(15) Sundaramurthi, D.; Krishnan, U. M.; Sethuraman, S. Electrospun Nanofibers as Scaffolds for Skin Tissue Engineering. *Polym. Rev.* **2014**, *54*, 348−376.
(16) Abrigo, M.; McArthur, S. L.; Kingshott, P. Electrospun Nanofibers as Dressings for Chronic Wound Care: Advances, Challenges, and Future Prospects. *Macromol. Biosci.* **2014**, *14*, 772−792.
(17) Yang, X.; Shah, J. D.; Wang, H. Nanofiber Enabled Layer-by-Layer Approach Toward Three-Dimensional Tissue Formation. *Tissue Eng., Part A* **2009**, *15*, 945−956.
(18) Mahjour, S. B.; Fu, X.; Yang, X.; Fong, J.; Sefat, F.; Wang, H. Rapid Creation of Skin Substitutes from Human Skin Cells and Biomimetic Nanofibers for Acute Full-Thickness Wound Repair. *Burns* **2015**, *41*, 1764−1774.
(19) Fu, X.; Xu, M.; Liu, J.; Qi, Y.; Li, S.; Wang, H. Regulation of Migratory Activity of Human Keratinocytes by Topography of Multiscale Collagen-Containing Nanofibrous Matrices. *Biomaterials* **2014**, *35*, 1496−1506.
(20) Huang, C.; Fu, X.; Liu, J.; Qi, Y.; Li, S.; Wang, H. The Involvement of Integrin B1 Signaling in the Migration and Myofibroblastic Differentiation of Skin Fibroblasts on Anisotropic Collagen-Containing Nanofibers. *Biomaterials* **2012**, *33*, 1791−1800.
(21) Venugopal, J.; Ramakrishna, S. Biocompatible Nanofiber Matrices for the Engineering of a Dermal Substitute for Skin Regeneration. *Tissue Eng.* **2005**, *11*, 847−854.
(22) Gautam, S.; Chou, C.-F.; Dinda, A. K.; Potdar, P. D.; Mishra, N. C. Surface Modification of Nanofibrous Polycaprolactone/Gelatin Composite Scaffold by Collagen Type I Grafting for Skin Tissue Engineering. *Mater. Sci. Eng., C* **2014**, *34*, 402−409.
(23) Trengove, N. J.; Stacey, M. C.; Macauley, S.; Bennett, N.; Gibson, J.; Burslem, F.; Murphy, G.; Schultz, G. Analysis of the Acute and Chronic Wound Environments: The Role of Proteases and Their Inhibitors. *Wound Repair Regen.* **1999**, *7*, 442−452.
(24) Lauer, G.; Sollberg, S.; Cole, M.; Krieg, I.; Eming, J.; Flamme, K.; Stürzebecher, T.; Mann, S. A. Expression and Proteolysis of Vascular Endothelial Growth Factor Is Increased in Chronic Wounds. *J. Invest. Dermatol.* **2000**, *115*, 12−18.
(25) Schneider, L. A.; Korber, A.; Grabbe, S.; Dissemond, J. Influence of PH on Wound-Healing: A New Perspective for Wound-Therapy? *Arch. Dermatol. Res.* **2007**, *298*, 413−420.
(26) Gainza, G.; Villullas, S.; Pedraz, J. L.; Hernandez, R. M.; Igartua, M. Advances in Drug Delivery Systems (DDSs) to Release Growth Factors for Wound Healing and Skin Regeneration. *Nanomed. Nanotechnol. Biol. Med.* **2015**, *11*, 1551−1573.
(27) Kim, H. S.; Sun, X.; Lee, J.-H.; Kim, H.-W.; Fu, X.; Leong, K. W. Advanced Drug Delivery Systems and Artificial Skin Grafts for Skin Wound Healing. *Adv. Drug Deliv. Rev.* **2019**, *146*, 209−239.
(28) Saghazadeh, S.; Rinoldi, C.; Schot, M.; Kashaf, S. S.; Sharifi, F.; Jalilian, E.; Nuutila, K.; Giatsidis, G.; Mostafalu, P.; Derakhshandeh, H.; Yue, K.; Swieszkowski, W.; Memic, A.; Tamayol, A.; Khademhosseini, A. Drug Delivery Systems and Materials for Wound Healing Applications. *Adv. Drug Deliv. Rev.* **2018**, *127*, 138−166.
(29) Meinel, A. J.; Germershaus, O.; Luhmann, T.; Merkle, H. P.; Meinel, L. Electrospun Matrices for Localized Drug Delivery: Current Technologies and Selected Biomedical Applications. *Eur. J. Pharm. Biopharm.* **2012**, *81*, 1−13.
(30) Stack, M. E. *Multifunctional, Biomimetic, Acellular Skin Grafts for the Treatment of Chronic, Diabetic Foot Ulcers*. Doctoral Dissertation, Stevens Institute of Technology, Hoboken, NJ, 2022.
(31) Yang, X.; Ogbolu, K. R.; Wang, H. Multifunctional Nanofibrous Scaffold for Tissue Engineering. *J. Exp. Nanosci.* **2008**, *3*, 329−345.
(32) Albright, V.; Xu, M.; Palanisamy, A.; Cheng, J.; Stack, M.; Zhang, B.; Jayaraman, A.; Sukhishvili, S. A.; Wang, H. Micelle-Coated, Hierarchically Structured Nanofibers with Dual-Release Capability for Accelerated Wound Healing and Infection Control. *Adv. Healthcare Mater.* **2018**, *7*, 1800132.
(33) Cordelires, F. *Manual Tracking*. https://imagej.nih.gov/ij/plugins/track/track.html.

https://doi.org/10.1021/acsami.2c13887
ACS Appl. Mater. Interfaces XXXX, XXX, XXX−XXX

(34) Thevenaz, P.; Ruttimann, U. E.; Unser, M. A Pyramid Approach to Subpixel Registration Based on Intensity. *IEEE Trans. Image Process.* **1998**, *7*, 27−41.
(35) Suarez-Arnedo, A.; Torres Figueroa, F.; Clavijo, C.; Arbeláez, P.; Cruz, J. C.; Muñoz-Camargo, C. An Image J Plugin for the High Throughput Image Analysis of in Vitro Scratch Wound Healing Assays. *PLoS One* **2020**, *15*, No. e0232565.
(36) Stirling, D. R.; Swain-Bowden, M. J.; Lucas, A. M.; Carpenter, A. E.; Cimini, B. A.; Goodman, A. CellProfiler 4: Improvements in Speed, Utility and Usability. *BMC Bioinf.* **2021**, *22*, 433.
(37) Pelton, R. W.; Saxena, B.; Jones, M.; Moses, H. L.; Gold, L. I. Immunohistochemical Localization of TGFβ1, TGFβ2, and TGFβ3 in the Mouse Embryo: Expression Patterns Suggest Multiple Roles during Embryonic Development. *J. Cell Biol.* **1991**, *115*, 1091−1105.
(38) Armbruster, D. A.; Pry, T. Limit of Blank, Limit of Detection and Limit of Quantitation. *Clin. Biochem. Rev.* **2008**, *29*, S49−S52.
(39) Pace, R. T.; Burg, K. J. L. Toxic Effects of Resazurin on Cell Cultures. *Cytotechnology* **2015**, *67*, 13−17.
(40) Bettinger, C. J.; Langer, R.; Borenstein, J. T. Engineering Substrate Topography at the Micro- and Nanoscale to Control Cell Function. *Angew. Chem., Int. Ed.* **2009**, *48*, 5406−5415.
(41) Jin, H.; Hong, Z.; Su, W.; Li, J. A Plant-Specific Calreticulin Is a Key Retention Factor for a Defective Brassinosteroid Receptor in the Endoplasmic Reticulum. *Proc. Natl. Acad. Sci.* **2009**, *106*, 13612−13617.
(42) Johnson, C. D. L.; D'Amato, A. R.; Gilbert, R. J. Electrospun Fibers for Drug Delivery after Spinal Cord Injury and the Effects of Drug Incorporation on Fiber Properties. *Cells Tissues Organs* **2016**, *202*, 116−135.
(43) Lin, K.; Chua, K.-N.; Christopherson, G. T.; Lim, S.; Mao, H.-Q. Reducing Electrospun Nanofiber Diameter and Variability Using Cationic Amphiphiles. *Polymer* **2007**, *48*, 6384−6394.
(44) Fon, D.; Zhou, K.; Ercole, F.; Fehr, F.; Marchesan, S.; Minter, M. R.; Crack, P. J.; Finkelstein, D. I.; Forsythe, J. S. Nanofibrous Scaffolds Releasing a Small Molecule BDNF-Mimetic for the Re-Direction of Endogenous Neuroblast Migration in the Brain. *Biomaterials* **2014**, *35*, 2692−2712.
(45) Woodard, L. N.; Grunlan, M. A. Hydrolytic Degradation and Erosion of Polyester Biomaterials. *ACS Macro Lett.* **2018**, *7*, 976−982.
(46) Chou, S.-F.; Carson, D.; Woodrow, K. A. Current Strategies for Sustaining Drug Release from Electrospun Nanofibers. *J. Controlled Release* **2015**, *220*, 584−591.
(47) Avila-Rodríguez, M.; Meléndez-Martínez, D.; Licona-Cassani, C.; Manuel Aguilar-Yañez, J.; Benavides, J.; Lorena Sánchez, M. Practical Context of Enzymatic Treatment for Wound Healing: A Secreted Protease Approach (Review). *Biomed. Rep.* **2020**, *13*, 3−14.
(48) McCarty, S. M.; Percival, S. L. Proteases and Delayed Wound Healing. *Adv. Wound Care* **2013**, *2*, 438−447.
(49) Singer, A. J.; Clark, R. A. F. Cutaneous Wound Healing. *N. Engl. J. Med.* **1999**, *341*, 738−746.
(50) Pandya, U. M.; Egbuta, C.; Abdullah Norman, T. M.; Chiang, C.-Y.; Wiersma, V. R.; Panchal, R. G.; Bremer, E.; Eggleton, P.; Gold, L. I. The Biophysical Interaction of the Danger-Associated Molecular Pattern (DAMP) Calreticulin with the Pattern-Associated Molecular Pattern (PAMP) Lipopolysaccharide. *Int. J. Mol. Sci.* **2019**, *20*, 408.
(51) Bays, J. L.; DeMali, K. A. Vinculin in Cell−Cell and Cell−Matrix Adhesions. *Cell. Mol. Life Sci.* **2017**, *74*, 2999−3009.
(52) Kim, D.-H.; Wirtz, D. Focal Adhesion Size Uniquely Predicts Cell Migration. *FASEB J.* **2013**, *27*, 1351−1361.
(53) Ridley, A. J. Life at the Leading Edge. *Cell* **2011**, *145*, 1012−1022.
(54) Stutchbury, B.; Atherton, P.; Tsang, R.; Wang, D.-Y.; Ballestrem, C. Distinct Focal Adhesion Protein Modules Control Different Aspects of Mechanotransduction. *J. Cell Sci.* **2017**, *130*, 1612−1624.
(55) Wozniak, M. A.; Modzelewska, K.; Kwong, L.; Keely, P. J. Focal Adhesion Regulation of Cell Behavior. *Biochim. Biophys. Acta* **2004**, *1692*, 103−119.
(56) Zhang, Y.; Guo, W.; Bi, M.; Liu, W.; Zhou, L.; Liu, H.; Yan, F.; Guan, L.; Zhang, J.; Xu, J. Migrasomes: From Biogenesis, Release, Uptake, Rupture to Homeostasis and Diseases. *Oxid. Med. Cell. Longev.* **2022**, *2022*, 4525778.
(57) Gold, L. I.; Eggleton, P.; Sweetwyne, M. T.; Van Duyn, L. B.; Greives, M. R.; Naylor, S.-M.; Michalak, M.; Murphy-Ullrich, J. E. Calreticulin: Non-endoplasmic Reticulum Functions in Physiology and Disease. *FASEB J.* **2009**, *24*, 665−683.
(58) Huttenlocher, A.; Horwitz, A. R. Integrins in Cell Migration. *Cold Spring Harbor Perspect. Biol.* **2011**, *3*, a005074.
(59) Repesh, L. A.; Fitzgerald, T. J.; Furcht, L. T. Fibronectin Involvement in Granulation Tissue and Wound Healing in Rabbits. *J. Histochem. Cytochem.* **1982**, *30*, 351−358.
(60) Zhang, K.; Kramer, R. H. Laminin 5 Deposition Promotes Keratinocyte Motility. *Exp. Cell Res.* **1996**, *227*, 309−322.

https://doi.org/10.1021/acsami.2c13887
ACS Appl. Mater. Interfaces XXXX, XXX, XXX−XXX